Rydberg Series of Dark Excitons in Cu_2O

Andreas Farenbruch,[1] Dietmar Fröhlich,[1] Dmitri R. Yakovlev,[1,2] and Manfred Bayer[1,2]
[1]Experimentelle Physik 2, Technische Universität Dortmund, D-44221 Dortmund, Germany
[2]Ioffe Institute, Russian Academy of Sciences, 194021 St. Petersburg, Russia

(Received 16 April 2020; accepted 5 October 2020; published 10 November 2020)

We demonstrate the Rydberg series of dark excitons, known as paraexcitons, up to the principal quantum number $n = 6$ for the yellow exciton series in Cu_2O, using second harmonic generation. Each of these states is optically inactive to all orders, but their observation becomes possible by application of a magnetic field which leads to mixing with the quadrupole-allowed bright excitons, called orthoexcitons, of the same n. The dark parastates are generally located below the bright orthostates, whose energies are increased by the electron-hole exchange interaction, except for $n = 2$, where this order is reversed. This inversion occurs due to band mixing, namely, of the $2S_{y,o}$ orthoexciton of the yellow series with the $1S_{g,o}$ orthoexciton of the green exciton series.

DOI: 10.1103/PhysRevLett.125.207402

Excitons attract strongly enhanced interest recently: a key factor is, for example, the emergence of 2D materials with exciton binding energies up to more than 100 meV, so that their optical properties are determined by excitonic features, even in ambient conditions [1,2]. A comprehensive understanding necessitates the observation of the excited states with principal quantum numbers $n > 1$ in an exciton series. The number of observed excited states has been limited: For the prototype direct band gap semiconductor GaAs, two excited states were measured at zero magnetic field [3], while for 2D materials the maximum n so far is 5 [4]. A remarkable exception is Cu_2O, for which excited states of the yellow exciton up to $n = 25$ were detected [5].

The universal feature in each of these cases is that the associated optical transitions are electric-dipole allowed, so that the excitons represent optically active states, also called "bright," even if excitable only in a higher-order process. Excitation of "dark" excitons would require a spin flip, therefore, they are optically inactive to all orders of perturbative treatment of the light-matter interaction. Because of the resulting long lifetime they are attractive, for example, for handling information, even on the quantum level [6], or accumulation in large numbers to achieve collective effects like a Bose-Einstein condensation [7,8].

Dark excitons can be optically activated by an external perturbation that induces a mixing with bright excitons. Most prominent is the application of a magnetic field which causes an exciton symmetry reduction. This has enabled dark exciton observation, if in addition the splitting from bright excitons by the electron-hole exchange interaction is large enough to separate them spectrally, for example, in quantum dots, where the exchange is enhanced by spatial confinement [9].

Also for Cu_2O the dark ground state exciton could be observed [10–12], facilitated by the strong Coulomb interaction in this material. Here, the dipole-allowed excitons have P-type envelope wave functions with orbital angular momentum $L = 1$, and their energies approximately follow a hydrogen series Ry/n^2, where $\mathrm{Ry} = 86$ meV. The P excitons form a subset of the orthoexcitons, whose entirety is completed by the states with orbital angular momenta $L \leq (n-1)$ different from unity. For the ground state $n = 1$ with the only possible value $L = 0$, the S orthoexciton is optically allowed in quadrupole approximation. Applying a magnetic field, the corresponding dark S paraexciton appears in absorption [10]. Below we use the terms bright and dark as well as ortho- and paraexciton equivalently for Cu_2O. In the Supplemental Material [13], we discuss their angular momentum configurations in detail.

In Cu_2O, like in any other material, the dark exciton observation has been restricted to the ground state. This raises the fundamental question about observability of excited dark excitons: We demonstrate here the Rydberg series of S paraexcitons in Cu_2O and measure their energies relative to the orthoexcitons. The latter point is closely related to the question, whether the dark exciton energies are generally located below the bright excitons as one may expect from Hund's rules, or whether there are deviations from this seemingly universal rule. So far, only one exception from the conventional order was reported: For perovskite nanocrystals the dark state was recently claimed to be above the bright state for the ground state exciton, which has been intensely debated since [17].

Using second harmonic generation (SHG) in magnetic field, we disclose the Rydberg series of paraexcitons up to $n = 6$. Compared to the 12 meV splitting between the $1S$ ortho- and paraexciton [10], the splittings for the excited states are on the order of a meV or fractions of it, in good agreement with calculations of Schweiner *et al.* [18].

Strikingly, while the paraexcitons are mostly located below the orthoexcitons, for $n = 2$ the order is reversed. According to Ref. [18], this can be traced to the mixing of the $2S_{y,o}$ yellow orthoexciton with the close-by $1S_{g,o}$ orthoexciton of the green series. Because of this mixing, the two levels repel each other so that the $2S_{y,o}$ orthoexciton is pushed in energy below the $2S_{y,p}$ paraexciton. Here, we used the subscripts y and g for yellow and green, o and p for ortho and para.

The difficulty in observing dark excitons is the dominance of bright excitons in optical spectra, be they allowed in electric-dipole or higher order. To resolve the dark states with relatively small oscillator strength, even when mixed with bright states by the magnetic field, one has to suppress the bright excitons, i.e., in one photon absorption the P excitons in Cu_2O as much as possible. To avoid them, we chose SHG spectroscopy as the experimental technique, where the even excitons can be resonantly excited by two photons combining two electric dipole transitions, followed by coherent emission of a photon with the exciton energy in a quadrupole transition [19]. The experimental setup is described in detail in Refs. [19,20]. As a light source we use an optical parametric amplifier pumped by a laser, emitting 200 fs pulses with tunable central photon energy at half the exciton energies. The pulse linewidth of 14 meV (full width at half maximum after frequency-doubling) allows recording of a spectrum across this energy range with a single laser setting, for which we can select between two spectrometers (80 or 20 μeV resolution).

The samples are placed in the He-4 insert (temperature of 1.4 K) of an optical magnetocryostat. Magnetic fields up to 10 T are applied in the Voigt geometry (magnetic field $\mathbf{B}$ perpendicular to light wave vector $\mathbf{k}$). The linear polarizations of laser light ($\mathbf{E}^{\omega}$) and SHG light ($\mathbf{E}^{2\omega}$) can be chosen by combining a Glan Thompson prism and a half-wave plate. The configurations with respect to optical and crystal axes as well as polarizations (see figure captions) are optimized for cleanest dark exciton signal. Here we are interested mainly in state energies; we discuss the relation of SHG configuration and intensity in the Supplemental Material [13].

The SHG potential for studying dark excitons is demonstrated for the $1S_{y,p}$ paraexciton in Fig. 1. The second derivatives of the SHG spectra, rather than the absolute intensities, are plotted there. This procedure highlights weak features with reliable information about their energies [21]. In Fig. 1, with increasing field the $1S_{y,o}$ orthoexciton shows the expected threefold splitting according to the magnetic quantum numbers $M = 0, \pm 1$. The paraexciton emerges 12.12 meV below the orthoexciton for fields higher than 2 T. Their field-induced mixing is manifested by the repulsion between states of the same symmetry, which are the paraexciton and the central orthoexciton in the multiplet having both $M = 0$; see Supplemental Material [13].

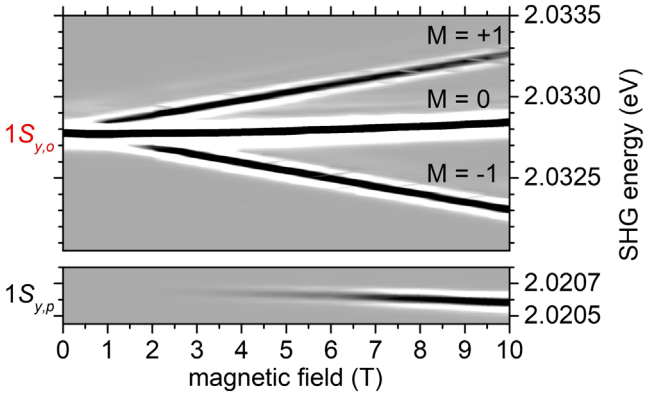

FIG. 1. Contour plot of second derivatives of SHG spectra in the $1S_{y,p}$ and $1S_{y,o}$ energy range (note the axis break) vs Voigt magnetic field. The central laser photon energy is set to half of 2.0206 for para- and 2.0328 eV for orthoexciton. Experimental configuration: $\mathbf{k}\|[111]$, $\mathbf{B}\|[1\bar{1}0]$, $\mathbf{E}^{\omega}$ at 45° to $\mathbf{B}$. For paraexciton $\mathbf{E}^{2\omega}$ is parallel to $\mathbf{B}$. For orthoexcitons $\mathbf{E}^{2\omega}$ is at 60° to $\mathbf{B}$ to observe the $M = 0$ as well as $M = \pm 1$ excitons [13]. For this setting, orthoexciton-SHG appears already at zero magnetic field.

Subsequently, we extend the SHG studies for the search of higher lying S-type paraexcitons of the yellow series. Identifying $n > 1$ parastates is complicated for the following reasons: (i) the decreasing exchange splitting by the increasing wave function extension, (ii) the reduced energy separation between excitonic shells nL, which in magnetic field split in a large number of lines so that they overlap already at quite low fields. Fortunately, due to the reduced exchange, weaker magnetic fields are required to induce mixing with the orthoexciton. As experimental hints for identifying para-energies, we use the following criteria: (a) emergence at energies below the orthoexciton, following the standard expectation; (b) no line splitting with increasing magnetic field; (c) weak magnetic field shift with indications for repulsion from associated S orthoexciton; (d) nonlinear increase of SHG intensity with magnetic field.

Figure 2(a) shows the magnetic field dependence of SHG spectra with the central laser photon energy at half of the $3S_{y,o}$ orthoexciton energy. Applying a magnetic field, SHG signal appears at small field strengths for each multiplet n at the energies of the S, P, and D states, as identified previously [21] so that we will not discuss them further. Of interest here are the energy ranges below the S states. Below the $3S_{y,o}$, starting from about 7 T, an additional line appears around 2.1594 eV, which fulfills the criteria formulated above. Therefore, we assign it to the $3S_{y,p}$ paraexciton, also, because in this range no other state is expected. For $n = 4$, the same signatures are found: At 1.5 T a single line appears below $4S_{y,o}$, which we assign to the $4S_{y,p}$ paraexciton.

For $n = 3$ the splitting between ortho- and paraexciton is 1.39 meV, while for $n = 4$ the splitting is reduced to 0.52 meV, where we extrapolate the paraexciton energy to

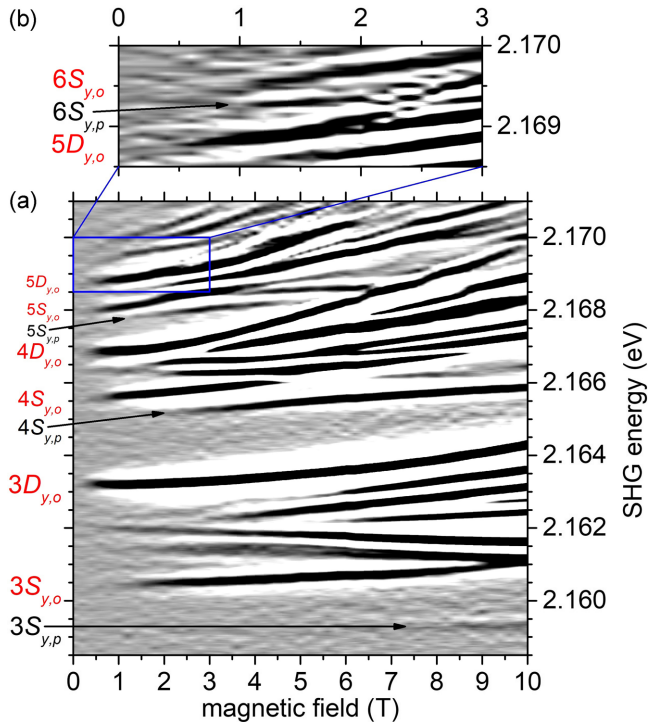

FIG. 2. Contour plots of SHG spectra vs magnetic field. (a) Shown are SHG second derivatives for energies from the $n = 3$ multiplet upwards. The central laser photon energy is set to half of 2.164 eV. Experimental configuration: $\mathbf{k}\|[1\bar{1}0]$, $\mathbf{B}\|[110]$, $\mathbf{E}^{\omega}\|\mathbf{B}$, $\mathbf{E}^{2\omega}\|[001]$. Then orthoexciton-SHG is forbidden at zero magnetic field, but emerges at finite B [20]. Further, only the $M = 0$ orthoexciton can be observed, see Supplemental Material [13]. (b) Fourth SHG derivatives around the $n = 5$ D states up to the $n = 6$ multiplet.

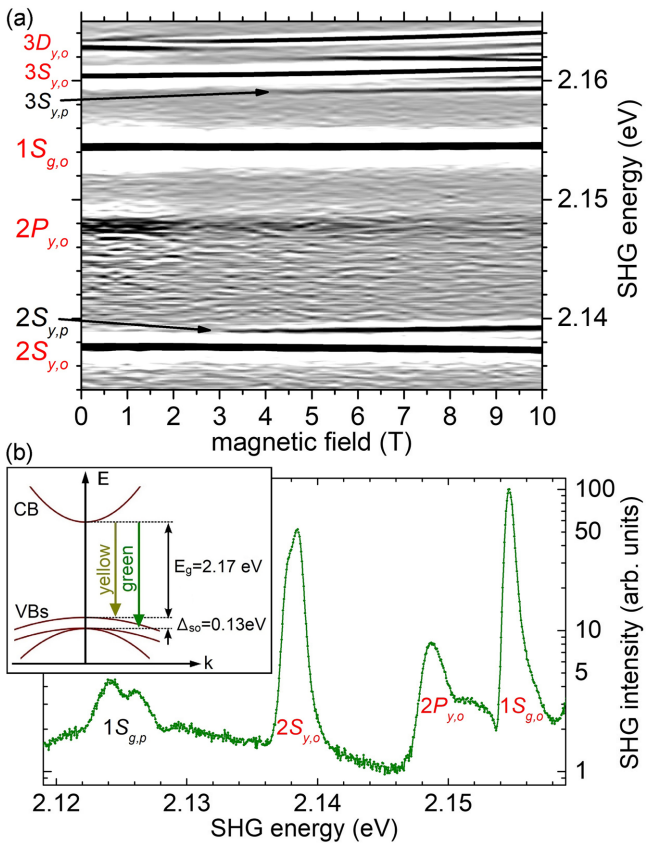

FIG. 3. (a) Contour plot of SHG spectra vs magnetic field in the $n = 2$ and 3 energy range. The laser photon energy is set to half of 2.138 eV in the configuration: $\mathbf{k}\|[111]$, $\mathbf{B}\|[11\bar{2}]$, $\mathbf{E}^{\omega}\|\mathbf{E}^{2\omega}\|\mathbf{B}$. Then orthoexciton SHG is allowed at zero magnetic field, but only the $M = 0$ state is observed, see Supplemental Material [13]. (b) SHG spectrum at $B = 10$ T, revealing the $1S_{y,p}$ paraexciton of the green series as doublet 30 meV below its orthoexciton. The laser photon energy was set to half of 2.125 eV. Experimental configuration: $\mathbf{k}\|[1\bar{1}0]$, $\mathbf{B}\|[001]$, $\mathbf{E}^{2\omega}\|\mathbf{B}$, $\mathbf{E}^{\omega}$ at 45° to $\mathbf{E}^{\omega}$. The sketch shows the conduction (CB) and valence bands (VBs) structure for the yellow and green excitons. Also band gap energy and VB splitting are given.

zero field using a B^2 dependence, see Supplemental Material [13]. For the $n = 5$ multiplet, interference with $n = 4$ states occurs for $B > 5$ T. For $B < 5$ T, below the $5S_{y,o}$ orthoexciton, a single, weakly shifting line appears, which is associated with the $5S_{y,p}$ paraexciton. Extrapolation to zero field gives an ortho-para splitting of 0.28 meV. Zooming in, one observes also the $6S_{y,p}$ paraexciton, see Fig. 2(b). B^2 extrapolation gives a splitting of 0.16 meV. Further data substantiating our observations are given in the Supplemental Material [13].

Finally, we turn to the $n = 2$ case. Corresponding SHG spectra are shown in Fig. 3(a) with the central photon energy at half of the $2S_{y,o}$ energy. In magnetic field an additional feature appears, which has to be associated with the $2S_{y,p}$ paraexciton, but surprisingly at higher energies than the orthoexciton. This is one of the exceptional cases where the dark exciton is located above the bright exciton. Extrapolating back to zero field, one obtains an ortho-para splitting of −1.27 meV.

The open squares in Fig. 4(a) show the measured splittings between ortho- and paraexcitons, $\Delta_n = E(nS_{\mathrm{y,o}}) - E(nS_{\mathrm{y,p}})$, vs the principal quantum number. The large $n = 1$ splitting of 12.12 meV is known from previous work [10] and reflects the small exciton size with strong Coulomb interaction. Also the $1S$ exciton binding energy of 150 meV is much larger than the Rydberg energy of 86 meV, derived from the P-exciton energies. For the states $n \geq 3$ the exchange splitting decreases with increasing n due to the increasing wave function extension.

The ortho-para splitting is determined by the short range exchange interaction [22,23], which is proportional to the square of the exciton envelope wave function for zero distance between electron and hole, $|\Psi_X(0)|^2$, scaling with principal quantum number as n^{-3} in a hydrogen-model [24,25]. Within the accuracy, the data for $n \geq 3$ are consistent with this scaling [Fig. 4(a)] but care has to be exercised here, see below. For completeness, we note that there are also paraexciton series for orbital angular

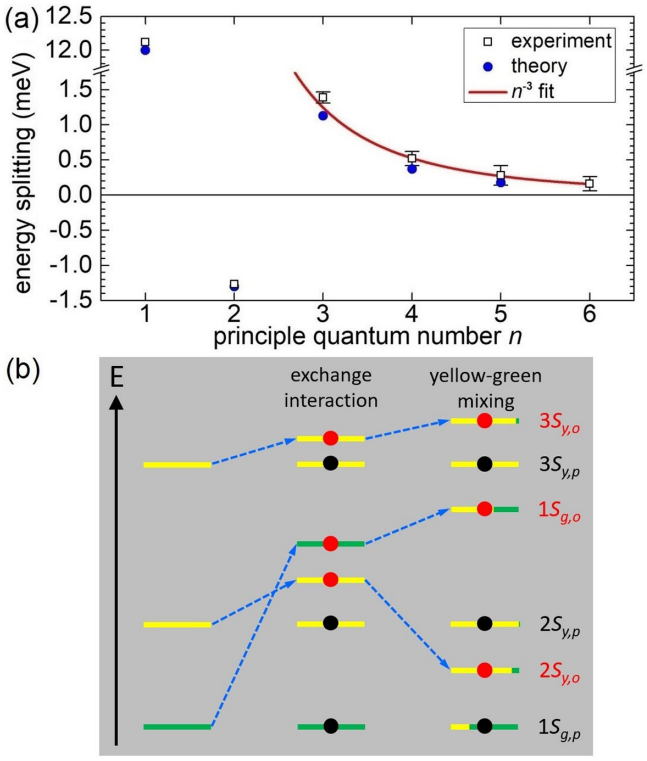

FIG. 4. (a) Energy splitting between ortho- and paraexcitons vs principal quantum number. Note the break on the ordinate axis. Squares give measured data, circles are from Ref. [18]. The red line is a fit with an n^{-3} dependence, using only data from $n = 4$ to 6. Error bars give the maximum tolerable deviation from the average energies determined through a least mean square fit. (b) Energy level scheme visualizing the exchange splitting between bright (red circles) and dark (black circles) excitons and the impact of band mixing. The energy levels are indicated by yellow (yellow excitons) and green (green excitons) bars. The relative green content due to band mixing is represented by the green part of the bar in the third column. Optical activity (inactivity) in zero magnetic field is marked by red (black) circles.

momenta $L > 0$. However, their splitting from the orthostates is small, as their envelope wave functions have nodes for zero electron-hole separation [26].

Our results for the energy splittings have to be compared with the calculations reported in Ref. [18], shown in Fig. 4 (a) by full circles. In this publication, the even ortho- and para-energies up to $n = 5$ were calculated. The agreement with experiment is quite good; see also Table I in the Supplemental Material [13]. We highlight that it was also predicted that for $n = 2$ the paraexciton is located at higher energies than the orthoexciton, but the origin was not discussed. The calculations show that the yellow exciton series, associated with transitions between the highest valence and lowest conduction band, cannot be treated isolated from the green exciton series. This series involves dipole forbidden transitions between the second highest valence and lowest conduction band, see scheme in Fig. 3(b). The $1S_{g,o}$ state of the green series with a binding energy of ≈150 meV, contributes prominently to the SHG spectrum in Fig. 3(a) as the intense line at 2.155 eV, about 16 meV above the yellow $2S_{y,o}$ orthoexciton.

When calculating the exciton levels, mixing effects between the valence bands need to be accounted for. The mixing is particularly relevant for the low lying excitons with small diameters, corresponding to a large spread in k space, and energetic proximity of the involved levels. For the excitons of interest here, only the $1S_{g,o/p}$ states of the green series are relevant, as the higher lying green states are located far apart in the yellow ionization continuum. The $1S_{g,o}$ orthoexciton is strongly admixed to the yellow $2S_{y,o}$ orthoexciton. Consequently, the two states repel each other. As a result, we attribute the dark-bright order reversal for $n = 2$ to the shift of the $2S_{y,o}$ orthoexciton to lower energies, beyond the energy of the dominantly yellow $2S_{y,p}$ paraexciton. Vice versa, the $1S_{g,o}$ exciton is moved to higher energies, as sketched in Fig. 4(b).

Schweiner *et al.* calculated the green content in the nominal yellow excitons [18]. The $2S_{y,o}$ state is 11% green, and the nominally green $1S_{g,o}$ state is 63% yellow, underlining their strong mixing, while the yellow $2S_{y,p}$ paraexciton is only 1.4% green. Mixing effects are also important for other states, however, with less drastic consequences. For example, for the $n = 3$ multiplet, located in energy above $1S_{g,o}$, the green content of the para- and orthostates is 0.5 and 4.5%, so that the orthostate will be pushed to higher energy, increasing the splitting from the parastate over the value expected if it had pure yellow character. Thus one has to be careful with deriving a scaling law with principal quantum number for the short range exchange, as it is strongly influenced by band mixing.

We also searched for the $1S$ paraexciton of the green series (the involved valence band is twofold degenerate at the Brillouin zone center, neglecting spin), for which indications were reported in Ref. [27]. The calculations of Schweiner *et al.* [18] predict a remarkably large splitting of the green ortho- and parastates of 30.8 meV. Performing experiments in the corresponding energy range reveals the $1S_{g,p}$, split by 1.5 meV into a doublet, see spectrum in Fig. 3(b). It indeed is located by slightly more than 30 meV below the green orthoexciton $1S_{g,o}$. The doublet splitting may be due to field-induced lifting of the valence band degeneracy.

In conclusion, we have demonstrated the Rydberg series of paraexcitons in Cu_2O up to $n = 6$ and determined the exchange splitting from the orthoexcitons, including a level inversion. Cu_2O is a unique system for studying excitons. However, understanding dark excitons is essential also for other materials due to their impact on the optical properties. Here we have shown a possible strategy for their observation which should be applicable to other systems, namely, optical activation due to mixing with bright excitons by a field-induced symmetry reduction, and

sensitive detection of the related weak signals using two-photon excitation techniques with selection rules different from optically active states in one-photon transitions. As band mixing is important for many materials, e.g., the heavy-light hole mixing in III–V and II–VI semiconductors, we expect also for them level inversions of bright and dark excitons.

We acknowledge the financial support by the Deutsche Forschungsgemeinschaft through the International Collaborative Research Centre TRR160 (Projects A8 and C8). We also acknowledge useful discussion with M. M. Glazov (Ioffe-Institute St. Petersburg) as well as P. Rommel and J. Main (University of Stuttgart).

[1] F. Xia, H. Wang, D. Xiao, M. Dubey, and A. Ramasubramaniam, Two-dimensional material nanophotonics, Nat. Photonics **8**, 899 (2014).

[2] W. Choi, N. Choudhary, G. H. Han, J. Park, D. Akinwande, and Y. H. Lee, Recent development of two-dimensional transition metal dichalcogenides and their applications, Mater. Today **20**, 116 (2017).

[3] G. W. Fehrenbach, W. Schäfer, J. Treusch, and R. G. Ulbrich, Transient Optical Spectra of a Dense Exciton Gas in a Direct-Gap Semiconductor, Phys. Rev. Lett. **49**, 1281 (1982).

[4] A. Chernikov, T. C. Berkelbach, H. M. Hill, A. Rigosi, Y. Li, O. B. Aslan, D. R. Reichman, M. S. Hybertsen, and T. F. Heinz, Exciton Binding Energy and Nonhydrogenic Rydberg Series in Monolayer WS_2, Phys. Rev. Lett. **113**, 076802 (2014).

[5] T. Kazimierczuk, D. Fröhlich, S. Scheel, H. Stolz, and M. Bayer, Giant Rydberg excitons in the copper oxide Cu_2O, Nature (London) **514**, 343 (2014).

[6] E. Poem, Y. Kodriano, C. Tradonsky, N. H. Lindner, B. D. Gerardot, P. M. Petroff, and D. Gershoni, Accessing the dark exciton with light, Nat. Phys. **6**, 993 (2010).

[7] D. W. Snoke and G. M. Kavoulakis, Bose-Einstein condensation of excitons in Cu_2O: Progress over 30 years, Rep. Prog. Phys. **77**, 116501 (2014).

[8] M. Beian, M. Alloing, R. Anankine, E. Cambril, C. G. Carbonell, A. Lemaitre, and F. Dubin, Spectroscopic signatures for the dark Bose-Einstein condensation of spatially indirect excitons, Europhys. Lett. **119**, 37004 (2017).

[9] M. Bayer, O. Stern, A. Kuther, and A. Forchel, Spectroscopic study of dark excitons in $In_xGa_{1-x}As$ self-assembled quantum dots by a magnetic-field-induced symmetry breaking, Phys. Rev. B **61**, 7273 (2000).

[10] J. Brandt, D. Fröhlich, Ch. Sandfort, M. Bayer, H. Stolz, and N. Naka, Ultranarrow Optical Absorption and Two-Phonon Excitation Spectroscopy of Cu_2O Paraexcitons in a High Magnetic Field, Phys. Rev. Lett. **99**, 217403 (2007).

[11] A. Mysyrowicz, D. P. Trauernicht, J. P. Wolfe, and H.-R. Trebin, Stress dependence of the paraexciton in Cu_2O, Phys. Rev. B **27**, 2562 (1983).

[12] G. Kuwabara, M. Tanaka, and H. Fukutani, Optical absorption due to paraexciton of Cu_2O, Solid State Commun. **21**, 599 (1977).

[13] See Supplemental Material at http://link.aps.org/supplemental/10.1103/PhysRevLett.125.207402 for more spectroscopic data, for a discussion of bright-dark inversion in polariton systems [14], for a summary table of experimental and theoretical data, for a group theoretical discussion of the exciton states [15,16], and for an explanation of the SHG polarization dependence.

[14] see, e.g., C. Gautham, M. Steger, D. Snoke, K. West, and L. Pfeiffer, Time-resolved two-photon excitation of long-lifetime polaritons, Optica **4**, 118 (2017).

[15] *Properties of the Thirty-Two Point Groups*, edited by G. F. Koster, J. O. Dimmock, R. G. Wheeler, and H. Statz (M.I.T. Press, Cambridge, MA, 1963).

[16] G. Dasbach, D. Fröhlich, R. Klieber, D. Suter, M. Bayer, and H. Stolz, Wave-vector-dependent exchange interaction and its relevance for the effective exciton mass in Cu_2O, Phys. Rev. B **70**, 045206 (2004).

[17] M. A. Becker, R. Vaxenburg, G. Nedelcu, P. C. Sercel, A. Shabaev, M. J. Mehl, J. G. Michopoulos, S. G. Lambrakos, N. Bernstein, J. L. Lyons, T. Stöferle, R. F. Mahrt, M. V. Kovalenko, D. J. Norris, G. Raino, and Al. L. Efros, Bright triplet excitons in caesium lead halide perovskites, Nature (London) **553**, 189 (2018).

[18] F. Schweiner, J. Main, G. Wunner, and C. Uihlein, Even exciton series in Cu_2O, Phys. Rev. B **95**, 195201 (2017).

[19] J. Mund, D. Fröhlich, D. R. Yakovlev, and M. Bayer, High-resolution second harmonic generation spectroscopy with femtosecond laser pulses on excitons in Cu_2O, Phys. Rev. B **98**, 085203 (2018).

[20] A. Farenbruch, J. Mund, D. Fröhlich, D. R. Yakovlev, M. Bayer, M. A. Semina, and M. M. Glazov, Magneto-Stark and Zeeman effect as origins of second harmonic generation on excitons in Cu_2O, Phys. Rev. B **101**, 115201 (2020).

[21] F. Schweiner, J. Main, G. Wunner, M. Freitag, J. Heckötter, C. Uihlein, M. Aßmann, D. Fröhlich, and M. Bayer, Magnetoexcitons in cuprous oxide, Phys. Rev. B **95**, 035202 (2017).

[22] V. A. Kiselev and A. G. Zhilich, Exchange and exchange-deformation splitting of exciton levels in a cuprous oxide crystal, Fiz. Tverd. Tela **13**, 2398 (1971) [Sov. Phys. Solid State **13**, 2008 (1972)]; M. M. Denisov and V. P. Makarov, Longitudinal and transverse excitons in semiconductors, Phys. Status Solidi B **56**, 9 (1973); G. E. Pikus and G. L. Bir, Exchange interaction in excitons in semiconductors, Zh. Eksp. Teor. Fiz. **60**, 195 (1971) [Sov. Phys. JETP **33**, 108 (1971)], http://www.jetp.ac.ru/cgi-bin/e/index/e/33/1/p108?a=list.

[23] G. M. Kavoulakis, Y.-C. Chang, and G. Baym, Fine structure of excitons in Cu_2O, Phys. Rev. B **55**, 7593 (1997) and references therein.

[24] J. Heckötter, M. Freitag, D. Fröhlich, M. Aßmann, M. Bayer, M. A. Semina, and M. M. Glazov, Scaling laws of Rydberg excitons, Phys. Rev. B **96**, 125142 (2017).

[25] We note that the short-range exchange has similarity with the hyperfine coupling of an electron to a nucleus, which is a contact interaction, so that its strength is as well proportional to the probability $|\Psi(0)|^2$ of finding the electron at the

nuclear site $\mathbf{R} = \mathbf{0}$. Using hydrogen wave functions one therefore also expects an n^{-3} dependence for the hyperfine interaction.

[26] Strictly speaking, for the even excitons, states with different L are mixed in the crystal due to spin-orbit interaction, so that the $D, G, \ldots$ excitons contain an S exciton component and are thus influenced by the exchange interaction, inducing a splitting of ortho- and parastates. We expect this splitting to be rather small, as it can occur starting from $n = 3$ only and the mixing is rather small. Therefore, we focus on the S paraexcitons, which we can clearly distinguish from the orthostates.

[27] V. T. Agekyan and Yu. A. Stepanov, Exchange-strain splitting and classification of the S exciton levels in cuprous oxide, Fiz. Tverd. Tela **17**, 1592 (1975) [Sov. Phys. Solid State **17**, 1041 (1975)].